Optimisation of glucose and levulinic acid production from the cellulose fraction of giant reed (*Arundo donax* L.) performed in the presence of ferric chloride under microwave heating

Nicola Di Fidio[1], Sara Fulignati[1], Isabella De Bari[2], Claudia Antonetti[1*], Anna Maria Raspolli Galletti[1]

[1] Department of Chemistry and Industrial Chemistry, University of Pisa, Via Giuseppe Moruzzi 13, 56124 Pisa, Italy.

[2] Laboratory for Processes and Technologies for Biorefineries and Green Chemistry, Italian National Agency for New Technologies, Energy and Sustainable Economic Development (ENEA), CR Trisaia, S.S. 106 Jonica, 75026 Rotondella (MT), Italy.

[*]Corresponding author: Claudia Antonetti

E-mail address: claudia.antonetti@unipi.it

Telephone: +39 0502219329

ABSTRACT

A two-step exploitation of the giant reed cellulose to glucose and levulinic acid, after the complete removal of the hemicellulose fraction, was investigated using $FeCl_3$ as catalyst. In the first step, the microwave-assisted hydrolysis of cellulose to glucose was optimised by response surface methodology analysis, considering the effect of temperature, reaction time and catalyst amount. Under the optimised reaction conditions, the glucose yield was 39.9 mol%. The cellulose-rich residue was also converted by enzymatic hydrolysis, achieving the glucose yield of 39.8 mol%. The

25   exhausted residue deriving from the chemical hydrolysis was further converted to

26   levulinic acid by microwave treatment at harsher reaction conditions. The maximum

27   levulinic acid yield was 64.3 mol%. On the whole, this cascade approach ensured an

28   extensive and sustainable exploitation of the C6 carbohydrates to glucose and levulinic

29   acid, corresponding to about 70 mol% of glucan converted to these valuable bioproducts

30   in the two steps.

31

32   **Keywords:** Giant reed; Glucose; Levulinic acid; $FeCl_3$; Response surface methodology.

33

34   **1. Introduction**

35   The employment of renewable resources as substrate for the production of added-

36   value compounds represents an urgent necessity due to the depletion of fossil

37   feedstocks. In particular, lignocellulosic biomass is one of the most promising

38   renewable resources, being mainly composed by three biopolymers (hemicellulose,

39   cellulose and lignin), all of them precursors of a wide range of valuable products and

40   innovative materials (Dutta et al., 2017; Kohli et al., 2019). On this basis, the

41   exploitation of each fraction is fundamental under the biorefinery perspective and a

42   cascade multi-step approach could ensure the highest valorisation of each macro-

43   compound. Hemicellulose is more easily hydrolysable than cellulose, requiring milder

44   reaction conditions for its conversion to xylose, whilst harsher reaction conditions are

45   necessary for the cellulose hydrolysis, but these last can also cause the C5 and C6

46   sugars successive conversion to furans and organic acids (Antonetti et al., 2019; Jeong

47   et al., 2017; Liao et al., 2018; Tempelman et al., 2019). These last compounds

48   represented mainly by levulinic acid (LA), formic acid (FA), 5-hydroxymethylfurfural

49   (HMF) and furfural, can be also valuable platform-chemicals for the production of

50   monomers, such as 2,5-furandicarboxylic acid, 2,5-bis(hydroxymethyl)furan, 2,5-

51   bis(hydroxymethyl)tetrahydrofuran, and maleic acid; solvents, such as

52   tetrahydrofurfuryl alcohol and 2-methyltetrahydrofuran; and biofuels, such as γ-

53   valerolactone and 2-butanol (Chen et al., 2018; Fulignati et al., 2019; Liao et al., 2018;

54   Liao et al., 2020; Licursi et al., 2018a; Matsagar et al., 2020; Van Nguyen et al., 2020).

55   However, in the sugars conversion through the fermentative route, they are often

56   microbial inhibitors (Kumar et al., 2019), and this implies that the choice of the most

57   suitable hydrolysis process and conditions is strongly dependent on the downstream

58   operation and on the target product. The hydrolysis of hemicellulose and cellulose

59   generally requires the employment of an acid catalyst which can be homogeneous, such

60   as mineral acids and inorganic salts, or heterogeneous, such as resins and zeolites

61   (Chung et al., 2018; Di Fidio et al., 2019a; Di Fidio et al., 2020; Mishra & Ghosh,

62   2020). The adoption of inorganic salts, in particular chlorides, in the last years, has

63   received great attention because they are more efficient than the heterogeneous

64   catalysts, safer, cheaper and more easily recoverable than mineral acids (Rodriguez

65   Quiroz et al., 2019). Among metal chlorides, $FeCl_3$ resulted one of the most promising

66   systems for the hydrolysis of polysaccharides to sugars (Loow et al., 2015). However,

67   up to now, it has been mainly used in the biomass pretreatment for the selective

68   hydrolysis of hemicellulose (Di Fidio et al., 2019a; Kamireddy et al., 2013; Kang et al.,

69   2013; Lin et al., 2019; Liu et al., 2009; Loow et al., 2015). In fact, recent works have

70   reported that the initial treatment with $FeCl_3$ efficiently hydrolysed the hemicellulose

71   fraction and left a solid residue more easily hydrolysable by enzymes (Lin et al., 2019).

72   Furthermore, Fe^{3+} ions displayed a positive influence on the enzymes activity (Wang et

73   al., 2018b) and finally, $FeCl_3$ is often employed in the preparation of culture media for

74   sugars fermentation (Saha et al., 2019). In this regard, when the sugars, produced in the

75   presence of the $FeCl_3$ catalyst, are exploited through the biological route, not only the

76   preliminary separation of this salt from the hydrolysates could result unnecessary, being

77   an essential component of the culture medium, but its presence can also improve the

78   following sugar conversion, avoiding the addition of fresh $FeCl_3$. On the contrary, when

79   the sugars are exploited through the chemical route, the separation and recycling of

80    $FeCl_3$ is an important step in order to reduce the capital costs. In this regard, $FeCl_3$ can

81   be recovered as ferric hydroxide that can be separated by ultrafiltration and

82   subsequently treated with HCl, in order to obtain again $FeCl_3$ available for a further

83   catalytic run (Kamireddy et al., 2013; Loow et al., 2015). Up to now, several biomasses

84   have been hydrolysed employing $FeCl_3$ aqueous solution, such as corn stover,

85   *Miscanthus* straw, rapeseed straw and, only recently, giant reed (*Arundo donax* L.) (Di

86   Fidio et al., 2019a; Kang et al., 2013; Liu et al., 2009). In particular, the latter is a very

87   promising biomass, being a perennial herbaceous plant characterised by a high content

88   of structural carbohydrates, about 60 wt%, and by a high production yield (30 t ha^{-1}

89   year^{-1}) (Dragoni et al., 2015). All these properties have driven the research towards its

90   chemical exploitation not only at the laboratory scale, but also for real industrial

91   applications, such as for the production of bioethanol through the Proesa$^®$ technology

92   developed by the joint venture between Biochemtex, Texas Pacific Group and

93   Novozymes (De Bari et al., 2013; Di Fidio et al., 2019b; Di Fidio et al., 2020; Licursi et

94   al., 2018b; Shatalov & Pereira, 2012). On the basis of its great potentialities, giant reed

95   and in particular its cellulose fraction was employed as feedstock of the present study.

96   In our previous work (Di Fidio et al., 2019a), the complete hydrolysis of the

hemicellulose fraction of giant reed (at a biomass loading of 9 wt%) was successfully

accomplished in the presence of $FeCl_3$ aqueous solution (1.6 wt%) by microwave

irradiation, achieving the highest xylose yield of 98.2 mol% together with the glucose

yield of 14.1 mol% at 150 °C for 2.5 min. The cellulose-rich residue (CRR) was then

separated and further treated with $FeCl_3$ to produce LA, giving the final LA yield of

57.6 mol%. A similar approach has been also investigated by other authors in the

literature (Di Fidio et al., 2019a; Wang et al., 2018a; Zheng et al., 2017). On the other

hand, glucose achievable through the hydrolysis of the starting CRR could be a versatile

platform for the production of many other bio-based products (Di Fidio et al., 2019b;

Silvester et al., 2019; Wang et al., 2019). Thus, it would be very interesting to optimise

the process in order to produce glucose and LA from CRR through a cascade approach

by the control of reaction conditions.

The present work aimed the stepwise exploitation of the cellulose remained in the

CRR, collected after the complete hydrolysis of giant reed hemicellulose, to give

glucose and then LA, through a microwave (MW)-assisted two-step approach. In the

first step, the synthesis of glucose in the presence of $FeCl_3$ was optimised through a

chemometric approach based on the response surface methodology (RSM) and the

results compared with those obtained in the more selective enzymatic hydrolysis,

performed employing the commercial enzyme Cellic[®] CTec2 (De Bari et al., 2013; Di

Fidio et al., 2020). In the second step, the solid residue recovered from the optimised

chemical conversion was further processed to LA, thus allowing a versatile exploitation

of the *A. donax* L. cellulose.

2. Materials and methods

2.1. Feedstock and materials

The Institute of Life Sciences Scuola Superiore Sant'Anna (Pisa, Italy) provided the raw giant reed collected and treated as already described in our previous work where its chemical composition is also reported (Di Fidio et al., 2019a). HMF (95%) was provided by AVA-Biochem. Glucose (>99%), xylose (>99%), furfural (99%), FA (99.8%), acetic acid (>99%), LA (98%), $FeCl_3 \cdot 6H_2O$ (>97%) were purchased by Sigma-Aldrich and employed as received. The enzyme Cellic® CTec2 was kindly provided by Novozymes.

2.2. Compositional analysis of the solids

The chemical composition of all solid residues was determined through the NREL protocols already adopted in our previous work (Di Fidio et al., 2020). The compositional analysis was performed in triplicate and the mean of data was reported together with the corresponding standard deviation.

2.3. X-ray Diffraction (XRD)

The powder XRD analysis was carried out by a Bruker D2 Phaser diffractometer (30 kV, 10 mA) operating in Bragg-Brentano geometry ($\theta - \theta$ scan mode) provided with a 1-dimensional Lynxeye detector. Ni-filtered Cu Kα radiation was employed. The adopted operating conditions and the procedure for the evaluation of the crystallinity index (CrI) were performed according to our previous work (Di Fidio et al., 2020).

2.4. Fourier transformation infrared spectroscopy (FT-IR)

The FT-IR analysis of the starting CRR and its chemical post-hydrolysis residue was performed by the Perkin-Elmer Spectrum Two spectrophotometer employed in

144   Attenuated Total Reflectance (ATR) mode. The operating conditions were carried out as

145   described in our previous work (Di Fidio et al., 2019a).

146   *2.5. Microwave-assisted chemical hydrolysis of the cellulose-rich residue catalysed by*

147   *FeCl₃*

148   The monomodal microwave reactor CEM Discover S-class System was employed to

149   perform the microwave-assisted FeCl$_3$-catalysed hydrolysis. The adopted procedures

150   were analogous to those reported in our previous study (Di Fidio et al., 2019a). Each

151   reaction was performed in triplicate and the associated error resulted within 5%.

152   *2.6. Statistical modelling*

153   The production of glucose was optimised through the RSM according to the Box-

154   Behnken design (BBD). Temperature (T), reaction time (t) and catalyst amount (cat)

155   were selected as independent variables of the model. The variation ranges of these

156   factors were set as follows: temperature (x_1), 120-190 °C; reaction time (x_2), 5-65 min;

157   catalyst amount (x_3), 0.2-4.8 wt%. The CRR loading of 9 wt% was a constant of the

158   model. The dimensionless and normalised factors, ranging between (-1; +1), were

159   defined as follows:

160      $x_1 = 2 \times [T(°C)\text{-}155]/(190\text{-}120)$ (1)

161      $x_2 = 2 \times [t(min)\text{-}35]/(65\text{-}5)$ (2)

162      $x_3 = 2 \times [cat(wt\%)\text{-}2.5]/(4.8\text{-}0.2)$ (3)

163   Design Expert 12 (12.0.1.0) Trial Version was adopted to elaborate the results

164   according to the RSM model. The generic equation representing the correlation between

165   the independent variables (x_1, x_2, x_3) and the response (*Y*) is reported in eq. 4:

166      $Y = \beta_0 + \sum \beta_i x_i + \sum \beta_{ij} x_i x_j + \sum \beta_{ii} x_i^2$ (4)

167 where β_0, β_i, β_{ij} and β_{ii} are the regression coefficients, calculated from the experimental

168 data by multiple regression using the least-squares method. The statistical significance

169 of the response values was established by Student's t-test. The statistical significance of

170 the model was defined by the statistical parameters, measuring the correlation (R^2) and

171 the Fisher's F-test.

172 *2.7. Enzymatic hydrolysis of the cellulose-rich residue*

173 The NREL protocol (Adney & Baker, 1996) was employed to evaluate the enzymatic

174 activity of the commercial enzyme Cellic® CTec2, which resulted 134.5 FPU/mL.

175 The enzymatic hydrolysis of CRR and giant reed (blank test) was conducted

176 according to our previous study (Di Fidio et al., 2019b). The biomass loading was 9

177 wt%. Each hydrolysis reaction and analytical determination was carried out in triplicate

178 and the experimental error related to the reaction was within 5%.

179 *2.8. High Performance Liquid Chromatography (HPLC)*

180 HPLC analysis of the obtained hydrolysates was performed by using HPLC Jasco

181 LC-2000 equipped with the Benson 2000-0 BP-OA column (7.8 mm × 300 mm × 10

182 μm) and the operating conditions were analogous to those reported in our previous work

183 (Di Fidio et al., 2019a). The concentration of each compound was assessed from

184 calibration curves obtained with standard solutions. The analysis of each standards

185 concentration and sample was performed in triplicate and the experimental error was

186 within 3%.

187 *2.9. Definitions*

188 The amount of hexahydrate ferric chloride salt (FeCl$_3$·6H$_2$O), adopted as catalyst,

189 was reported as:

190 $$FeCl_3\ (wt\%) = \left[\left(0.6 \times m_{FeCl_3 \cdot 6H_2O}\right)/\left(m_{H_2O} + m_{FeCl_3 \cdot 6H_2O}\right)\right] \times 100 \tag{5}$$

191 where 0.6 is the ratio between the molecular weight values of ferric chloride and ferric

192 chloride hexahydrate, $m_{FeCl_3 \cdot H_2O}$ and m_{H_2O} are the amounts in grams (g) of ferric chloride

193 hexahydrate and water, respectively.

194   The substrate loading (SL) was calculated as:

195 $$\text{SL (wt\%)} = \left[m_s / \left(m_s + m_{H_2O} \right) \right] \times 100 \qquad (6)$$

196 where m_s and m_{H_2O} are the amounts (g) of the substrate and H_2O, respectively.

197   The amount m_i of the different compounds was obtained as follows:

198 $$m_i = c_i \times V \qquad (7)$$

199 where c_i is the compound concentration (g/L) and V is the volume (L).

200   The glucose yield (mol%) respect to the glucan moles of the CRR, was calculated

201 according to the following equation (Zhang et al., 2015):

202 $$\text{Glucose yield (mol\%)} = [(m_g \times 0.90)/(m_{CRR} \times G_{CRR}/100)] \times 100 \qquad (8)$$

203 where m_g is the glucose amount (g), 0.90 is the ratio between the molecular weight

204 values of the glucan monomer and the glucose, m_{CRR} is the mass (g) of the CRR

205 employed as substrate, G_{CRR} is the percentage of glucan in the dry CRR (wt%).

206   The LA yield (mol%) respect to the glucan moles of the solid residue, obtained from

207 the chemical hydrolysis of the cellulose fraction of the CRR, was calculated as follows:

208 $$\text{LA yield (mol\%)} = \left[(m_{LA} \times 1.40)/(m_r \times G_r/100) \right] \times 100 \qquad (9)$$

209 where m_{LA} is the LA amount (g), 1.40 is the ratio between the molecular weight values

210 of the glucan monomer and the LA, m_r is the mass (g) of the solid residue employed as

211 substrate, G_r is the percentage of glucan in the dry solid residue (wt%).

212   The substrate solubilisation was calculated according to the following equation:

213 $$\text{Substrate solubilisation (wt\%)} = 100 - (SR/SS) \times 100 \qquad (10)$$

where SR is the dried solid residue (g) obtained at the end of the hydrolysis and SS is

the adopted starting substrate (g) loaded in the microwave reactor.

The mass balance (wt%) was defined as follows:

$$\text{Mass balance (wt\%)} = ((\sum m_i + m_r)/m_{CRR}) \times 100 \qquad (11)$$

where m_i is the mass of each different product in the hydrolysate (g), m_r is the mass of

the post-reaction residue (g), m_{CRR} is the mass (g) of the CRR employed as substrate.

The turnover number (TON) was defined as follows:

$$\text{TON} = mol_s / mol_{cat} \qquad (12)$$

where mol_s is the moles of consumed substrate (glucan) and mol_{cat} is the moles of the

employed $FeCl_3$.

The turnover frequency (TOF) was defined as follows:

$$\text{TOF} = TON / t \qquad (13)$$

where TON is the turnover number and t is the reaction time in seconds.

3. Results and discussion

3.1. Optimisation of microwave-assisted FeCl₃-catalysed hydrolysis of the cellulose-

rich residue to glucose

In the present study, the giant reed CRR, recovered after the selective removal of

hemicellulose (Di Fidio et al., 2019a), was adopted as starting material for the cascade

exploitation of its cellulose fraction to glucose and LA. The CRR represented the 57.8

wt% of the starting giant reed and its chemical composition is reported in Table 1.

(Table 1, near here)

The microwave-assisted hydrolysis of CRR to glucose by $FeCl_3$ was optimised by a

multivariate analysis, according to the Box-Behnken design. Temperature (x_1), reaction

238   time (x_2) and FeCl$_3$ amount (x_3) were selected as independent variables of the model,

239   due to their synergistic effect on the glucose yield (mol%), which was the dependent

240   one. On the basis of the results achieved in our previous work, the CRR loading was

241   kept constant at 9 wt% (Di Fidio et al., 2019a). Table 2 reports the dimensionless and

242   dimensional factors selected in this investigation and the experimental values of glucose

243   yields. Table 3 shows the results in terms of products concentrations (g/L), mass

244   balance (wt%) and CRR solubilisation (wt%).

245   (Tables 2 and 3, near here)

246   According to Table 2, the highest glucose yields were reached under reaction

247   conditions characterised by an intermediate severity (runs 10, 13, 14 and 15), namely at

248   155 °C, 5 min, 4.8 wt% FeCl$_3$ (run 10) and 155 °C, 35 min, 2.5 wt% FeCl$_3$ (runs 13, 14

249   and 15). In fact, working with too mild reaction conditions (runs 1, 2, 5, 6, 9, 11),

250   namely at relatively low temperature of 120 °C (runs 1, 2, 5 and 6) or at 155 °C but in

251   the presence of relatively low catalyst amount of 0.2 wt% (runs 9 and 11), the chemical

252   hydrolysis of cellulose was scarcely activated, as evidenced by the obtained glucose

253   yields lower than 18.8 mol% and by the low CRR solubilisations (Tables 2 and 3). On

254   the other hand, the employment of too harsh reaction conditions (runs 3, 4, 7, 8, 12),

255   namely at relatively high temperature of 190 °C (runs 3, 4, 7 and 8) or at 155 °C but in

256   the presence of relatively high catalyst amount of 4.8 wt% (run 12), had a detrimental

257   influence on the glucose yields, again lower than 18.1 mol%, due to its degradation to

258   LA, FA and humins, as shown by the increase of rehydration acids concentration and

259   the decrease of the mass balance.

260   Regarding the statistical modelling of data, Table 4 reports the values calculated for

261   the set of regression coefficients involved in the equation 4, which describes the glucose

262 yield (Y) as a function of the main reaction parameters (x_1, x_2, x_3), together with their

263 statistical significance. In the same Table the significance and the correlation of the

264 model were described by the statistical Fisher's F and R^2 parameters, respectively.

265 (Table 4, near here)

266 The calculated coefficients for glucose yield indicated that it was positively affected

267 by temperature and catalyst amount, whereas the temperature-catalyst amount and

268 reaction time-catalyst amount interaction terms, which were the most influential ones,

269 negatively influenced the glucose yield. The model equation obtained from the Box-

270 Behnken design based on equation 4 results the following one:

271 $Y = 38.967 + 0.175x_1 - 1.8E^{-15}x_2 + 1.050x_3 - 2.225x_1x_2 - 6.225x_1x_3 - 5.975x_2x_3 - 0.526x_1^2 -$

272 $-24.221x_2^2 - 7.371x_3^2$

273 Figure 1A shows the dependence of the glucose yield on the reaction time and $FeCl_3$

274 amount at intermediate temperature ($x_1 = 0$), Figure 1B shows the dependence of

275 glucose yield on temperature and $FeCl_3$ amount at intermediate reaction time ($x_2 = 0$)

276 and finally Figure 1C shows the dependence of glucose yield on temperature and

277 reaction time at the intermediate $FeCl_3$ amount ($x_3 = 0$).

278 (Figure 1, near here)

279 The highest glucose yields (about 40 mol%) were predicted in the center of the response

280 curves reported in Figure 1, corresponding to reaction conditions of intermediate

281 severity, whereas at the extremes of these curves, namely in the presence of relatively

282 low or high values of temperature (120, 190 °C), reaction time (5, 65 min) and catalyst

283 amount (0.2, 4.8 wt%), the glucose yields strongly decreased. In fact, on the one hand,

284 the harsh conditions (190 °C, 65 min, 4.8 wt% $FeCl_3$) favoured the further dehydration

285 and degradation of glucose to LA, FA and humins, according to previous studies

(Antonetti et al., 2017). On the other hand, milder conditions (120 °C, 5 min, 0.2 wt% $FeCl_3$) did not promote the cellulose hydrolysis to glucose. On this basis, it is clear that since glucose is the intermediate product between the hydrolysis of cellulose and its conversion to LA, reaction conditions of intermediate severity are necessary to maximise the glucose production, limiting the formation of successive other products.

The model predicted the highest glucose yield of 39.0 mol% working at 155 °C for 34 min with 2.7 wt% $FeCl_3$. In order to validate the model, the reaction was carried out in triplicate under the predicted reaction conditions. The experimental glucose yield of 39.9 ± 0.9 mol% was reached, confirming the good prediction of the model. In addition, under the optimised reaction conditions the TON and TOF were 0.97 and $4.7 \cdot 10^{-4}$ s^{-1}, respectively. It is important to highlight that the optimised reaction conditions were even milder than those adopted in other studies for the hydrolysis of hemicellulose fraction of sugarcane bagasse and *Miscanthus* straw catalysed by $FeCl_3$ (Chen et al., 2014; Kang et al., 2013), despite the cellulose hydrolysis usually requires harsher reaction conditions than hemicellulose. In addition, the achieved hydrolysate had a concentration of 1.3 g/L HMF which could be tolerated by many microorganisms, thus making the hydrolysate potentially employable in biotechnological conversions (Asada et al., 2015). Furthermore, it is noteworthy that the optimised reaction conditions involves the employment of relatively low amount of $FeCl_3$, which enables the direct employment of the synthesised hydrolysate as substrate in subsequent bioconversion steps based on salt-tolerant microorganisms, such as *Saccharomyces cerevisiae* BA11 for the bio-ethanol production (Asada et al., 2018).

In the literature several studies reported the employment of $FeCl_3$ as catalyst for the hemicellulose hydrolysis, whereas the subsequent cellulose hydrolysis was usually

310 performed by enzymes (Kang et al., 2013; Liu et al., 2009; López-Linares et al., 2013).

311 Our investigation adopted an innovative approach based on the use of $FeCl_3$ as catalyst

312 for the conversion of the cellulose fraction of giant reed to glucose, the same catalyst

313 alredy reported for the hydrolysis of hemicellulose (Di Fidio et al., 2019a).

314 Furthermore, in order to assess the efficacy of the $FeCl_3$-catalysed hydrolysis of CRR,

315 the chemical route was compared to the biological one, based on the use of hydrolytic

316 enzymes, which is typically more selective.

317 *3.2. Enzymatic hydrolysis of the cellulose-rich residue to glucose*

318 Enzymatic hydrolysis is a very common approach for the selective hydrolysis of

319 polysaccharides to sugars. In the present work, the conversion of the cellulose fraction

320 of CRR to glucose was performed by enzymatic hydrolysis employing the commercial

321 enzyme Cellic® CTec2 and the obtained results are reported in Figure 2.

322 (Figure 2 near here)

323 The substrate loading of 9 wt% was adopted as already employed for chemical

324 hydrolysis and in agreement with our previous work (Di Fidio et al., 2020), in order to

325 achieve a relevant glucose concentration in the hydrolysate, thus favouring the process

326 scale-up and the economic sustainability of the reaction. The effect of the enzyme

327 dosage on its activity was investigated by comparing two different enzyme

328 concentrations, 15 and 25 FPU/g glucan. These values are lower than those employed in

329 the literature for the pretreated giant reed hydrolysis, generally higher than 60 FPU/g

330 glucan (Aliberti et al., 2017; Shatalov & Pereira, 2012), but they are in agreement with

331 the typical ranges reported for the hydrolysis of other lignocellulosic biomasses, such as

332 cardoon and wastepaper (Cotana et al., 2015; Wang et al., 2012). As shown in Figure 2,

333 in all the reactions, the glucose yield increased during the whole investigated reaction

334   time. In the presence of 15 FPU/g glucan Cellic® CTec2, the glucose yield reached 31.7

335   mol% at the end of the reaction. Increasing the enzyme amount to 25 FPU/g glucan, the

336   glucose yield improved, achieving 39.8 mol% after the same reaction time.

337   In order to demonstrate the beneficial role of the selective hemicellulose hydrolysis

338   step (Di Fidio et al., 2019a) on the substrate reactivity toward the subsequent enzymatic

339   hydrolysis, two comparison tests were performed under the same reaction conditions,

340   employing the raw giant reed as substrate. In the reference test with 15 FPU/g glucan,

341   the maximum glucose yield of 10.4 mol%, was observed at the end of the reaction.

342   When the Cellic® CTec2 amount was enhanced to 25 FPU/g glucan, the glucose yield,

343   after the same reaction time, raised to 16.6 mol%. The cellulose conversion was lower

344   than that achieved after the hemicellulose removal, proving the crucial role of

345   hemicellulose in limiting the enzymatic digestibility of cellulose. On the other side, the

346   cellulose hydrolysis was not quantitative even after the hemicellulose conversion,

347   probably due to the composition of the starting substrate. In fact, when lignocellulosic

348   biomass is the feedstock of the process, the enzyme activity is significantly affected by

349   the cellulose crystallinity and polymerisation (Lin et al., 2020), the fibers porosity and

350   size in the pretreated biomass (Zhang et al., 2014), the accessibility and hydrophobicity

351   of the substrate (Huang et al., 2019) and also by the presence of lignin (De Bari et al.,

352   2013; Huang et al., 2019; Lin et al., 2020). This latter hampers the specific interaction

353   of enzymes with the polysaccharides and could form inactive lignin-enzyme complexes,

354   which may involve both the insoluble and soluble low-molecular weight lignin,

355   reducing, in this way, the enzyme activity (Berlin et al., 2006). Nevertheless, the

356   glucose concentration of 21.8 g/L achieved starting from the pretreated giant reed in the

357   presence of 25 FPU/g glucan of enzyme was similar to the value of 24.8 g/L

accomplished by Aliberti et al. (Aliberti et al., 2017), who adopted the same loading of pretreated *A. donax* L. (9 wt%), but with a higher Cellic® CTec2 amount (34.8 FPU/g glucan) than that employed in this study.

The solid residue recovered after the enzymatic hydrolysis at the highest enzymes dosage (25 FPU/g glucan) was 77.3 wt% of CRR and its chemical composition is reported in Table 1. This chemical composition resulted similar respect to the one obtained by MW-assisted $FeCl_3$-catalysed hydrolysis under the optimised reaction conditions.

Considering the similar glucose concentration and yield achieved in the two different approaches, the catalyst cost and the involved reaction time, the chemical route resulted more efficient and sustainable than the biological one. Moreover, the chemical route offered the possibility of developing an overall conversion process more homogenous in terms of implemented technologies and more affordable in terms of catalysts cost and reaction time. For these reasons, the production of LA and FA was performed starting from the post chemical-hydrolysis residue, although the same approach is also possible using as substrate the solid residue obtained by the biological route.

3.3. Characterisation of the residue obtained from the optimised chemical hydrolysis of CRR

After the selective cellulose chemical-hydrolysis of CRR to glucose performed under the optimised reaction conditions, the solid residue was recovered. It represented the 56.1 wt% of the starting CRR and its chemical composition is reported in Table 1. The composition still confirmed the presence of cellulose in the solid residue. In order to investigate the effect of the microwave-assisted $FeCl_3$-catalysed hydrolysis on the crystallinity index (CrI) of the substrate, the X-ray Diffraction (XRD) analysis was

382 performed on the CRR and on the post chemical-hydrolysis residue. The CrI value of

383 the raw giant reed was determined in a previous work and it resulted 53.8% (Di Fidio et

384 al., 2020). After the complete and selective $FeCl_3$-catalysed hemicellulose hydrolysis

385 performed in our previous work (Di Fidio et al., 2019a), the CrI of the CRR slightly

386 decreased to 48.9%, indicating that, during the hydrolysis of hemicellulose, the

387 crystalline structure was not strongly damaged. Finally, after the chemical conversion of

388 CRR into glucose carried out under the above optimised reaction conditions, the CrI of

389 the final solid residue further decreased to 41.2%, confirming the efficacy of the

390 proposed process in the cellulose destructuration and dissolution.

391   The CRR and the post chemical-hydrolysis residue were also characterised by FT-IR

392 analysis. The bands at 2912 and 2841 cm^{-1}, corresponding to the C-H stretching of the -

393 OCH_3 group in the lignin (Chen et al., 2019), were more intense in the post chemical-

394 hydrolysis residue respect to the CRR. Also the peaks at 1708 and 1598 cm^{-1}, ascribed

395 to the C=O conjugated to the aromatic rings of lignin and to the aromatic skeletal in

396 lignin, respectively (Chen et al., 2019), were more sharp in the post chemical-hydrolysis

397 residue. Other well-defined bands in the post chemical-hydrolysis residue were those at

398 1455 and 1419 cm^{-1}, characteristic of the C=C stretching of benzene rings in lignin

399 (Licursi et al., 2015); that at 1101 cm^{-1}, assigned to the C-H deformation in the aromatic

400 skeletal of lignin (Licursi et al., 2015); those at 1056 and 1034 cm^{-1}, typical of C–O–C

401 stretching of the pyranose ring in cellulose and of the C–O stretching of hydroxyl and

402 ether groups of cellulose, respectively (Di Fidio et al., 2020). These observations proved

403 the partial removal of cellulose from the CRR and the enrichment of lignin in the post

404 chemical-hydrolysis residue.

405   *3.4. Production of LA from the residual cellulose of the post chemical-hydrolysis*

406   *residue*

407   LA was produced by the FeCl$_3$ treatment of the residue recovered from the optimised

408   chemical hydrolysis of CRR, working at harsh reaction conditions chosen on the basis

409   of our previous results, 190 °C, 2.4 wt% FeCl$_3$ with the substrate loading of 9 wt% (Di

410   Fidio et al., 2019a). The influence of the reaction time on the LA synthesis was

411   investigated and the obtained results are shown in Figure 3.

412   (Figure 3, near here)

413   The highest LA yield of 64.3 mol% together with the FA yield of 86.3 mol%,

414   corresponding to the concentrations of 18.4 and 9.8 g/L respectively, were reached after

415   15 min. In fact, at shorter reaction time (5 min), the LA yield was lower (60.2 mol%),

416   while the increase of the reaction time up to 45 min negatively affected the LA yield,

417   which decreased to 60.6 mol%, due to the humins formation. On this basis, the reaction

418   time of 15 min was selected as the optimal reaction time value for the production of

419   levulinic acid. TON and TOF values of 1.4 and 1.6 10^{-3} s^{-1}, respectively, were reached.

420   The obtained LA yield was significantly higher than the value of 48.5 mol% obtained

421   by Wang et al. starting from pretreated corncob (Wang et al., 2018a), despite they

422   worked with a lower substrate loading (4 wt%) than that adopted in the present study (9

423   wt%), with similar FeCl$_3$ amount (2 wt%) and with longer reaction time (120 min), the

424   latter probably due to the employment of traditional heating system instead of

425   microwave irradiation, as in the present work. Moreover, under their optimal reaction

426   conditions, the TON was about 0.6, which resulted about the half than that adopted in

427   the present study. The TOF was not comparable due to the different heating system

428   which significantly affects the reaction time. The obtained LA yield was also higher

than that reached by Zheng et al. from the direct conversion of corn stalk to LA

catalysed by $FeCl_3$ solutions, which was equal to about 49.0 mol% with a TON of about

0.3 (Zheng et al., 2017). Furthermore, it is worthwhile to highlight that the

accomplished LA yield was similar to that reported in the HCl-catalysed conversion of

raw giant reed to LA carried out under microwave heating (Licursi et al., 2018b),

demonstrating the efficiency of $FeCl_3$ as a valid alternative to strong and corrosive

acids. Moreover, in the study of Licursi et al. (Licursi et al., 2018b), the TON was 0.3,

about 5-folds lower than the value obtained in the present work, thus confirming the

promising performance of $FeCl_3$ for LA production. In addition, considering the

reaction time of 20 min under microwave heating, the TOF obtained by Licursi et al.

resulted about $2.5 \cdot 10^{-4}$ s^{-1}, which was lower than that achieved in the present work

$(1.6 \cdot 10^{-3}$ $s^{-1})$.

The solid residue recovered at the end of the entire cascade exploitation represented the

65.0 wt% of the post chemical-hydrolysis residue and its chemical composition is

shown in Table 1. The mass balance flow diagram of the chemical and enzymatic

processes from CRR is reported in Figure 4.

(Figure 4, near here)

These results confirmed the extensive exploitation of cellulose present in the CRR

into glucose and LA through the two-step MW-approach proposed in the present work,

achieving the cellulose conversion of 94.1 mol% and an overall yield of glucose and

LA, obtained in the first and in the second step respectively, of about 70 mol%. This

value resulted significantly higher respect to the yield of about 49 mol% reported in the

literature for the $FeCl_3$-catalysed direct conversion of glucan to LA starting from

corncob and corn stalk residues, recovered after the hemicellulose removal (Zheng et

453 al., 2017). Moreover, the attained overall yield was slightly higher than the value of

454 65.9 mol% achieved by Jeong and co-workers (Jeong et al., 2017) in the sulphuric acid-

455 catalysed direct conversion of glucan to LA starting from *Quercus mongolica* residue,

456 recovered after the hemicellulose dissolution.

457   Considering the entire process from the raw giant reed, our proposed multi-step

458 approach allowed the extensive valorisation of xylan and glucan components with the

459 same catalyst properly tuning the reaction conditions, thus leaving a lignin-rich solid

460 residue (acid-insoluble lignin 85.3 wt%) for the successive conversion of this last

461 component, aiming to the complete biomass valorisation.

462

463 **4. Conclusions**

464   This work investigated, for the first time, the employment of $FeCl_3$ for the

465 microwave-assisted two-step exploitation of the giant reed cellulose fraction to glucose

466 and LA, after the complete hydrolysis of hemicellulose. In the first step, the glucose

467 production was optimised by response surface methodology analysis, reaching the

468 highest yield of 39.9 mol%, similar to that obtained by the enzymatic hydrolysis. In the

469 second step, the LA yield of 64.3 mol% was achieved. This proposed cascade approach

470 resulted versatile and sustainable, ensuring the significant exploitation of the giant reed

471 cellulose fraction (about 70 mol% of glucan) to different valuable bioproducts.

472

484

485 **Appendix A. Supplementary data**

486 E-supplementary data of this work can be found in online version of the paper.

487

488 **References**

489 1. Adney, B., Baker, J., 1996. Measurement of cellulase activities. Laboratory

490 analytical procedure 6, 1996.

491 2. Aliberti, A., Ventorino, V., Robertiello, A., Galasso, M., Blaiotta, G., Comite, E.,

492 Faraco, V., Pepe, O., 2017. Effect of Cellulase, Substrate Concentrations, and

493 Configuration Processes on Cellulosic Ethanol Production from Pretreated Arundo

494 donax. Bioresources 12, 5321-5342.

495 3. Antonetti, C., Fulignati, S., Licursi, D., Raspolli Galletti, A.M., 2019. Turning Point

496 toward the Sustainable Production of 5-Hydroxymethyl-2-furaldehyde in Water:

497 Metal Salts for Its Synthesis from Fructose and Inulin. ACS Sustain. Chem. Eng. 7,

498 6830-6838.

499   4. Antonetti, C., Raspolli Galletti, A.M., Fulignati, S., Licursi, D., 2017. Amberlyst A-

500   70: A surprisingly active catalyst for the MW-assisted dehydration of fructose and

501   inulin to HMF in water. Catal. Commun. 97, 146-150.

502   5. Asada, C., Sasaki, C., Oka, C., Nakamura, Y., 2018. Ethanol Production from

503   Sugarcane Bagasse Using Pressurized Microwave Treatment with Inorganic Salts

504   and Salt-Tolerant Yeast. Waste Biomass Valorization 11, 1-7.

505   6. Asada, C., Sasaki, C., Takamatsu, T., Nakamura, Y., 2015. Conversion of steam-

506   exploded cedar into ethanol using simultaneous saccharification, fermentation and

507   detoxification process. Bioresour. Technol. 176, 203-209.

508   7. Berlin, A., Balakshin, M., Gilkes, N., Kadla, J., Maximenko, V., Kubo, S., Saddler,

509   J., 2006. Inhibition of cellulase, xylanase and β-glucosidase activities by softwood

510   lignin preparations. J. Biotechnol. 125, 198-209.

511   8. Chen, B., Wang, X., Leng, W., Mei, C., Zhai, S., 2019. Spectroscopic/Microscopic

512   Elucidation for Chemical Changes During Acid Pretreatment on *Arundo donax*. J.

513   Bioresour. Bioprod. 4, 192-199.

514   9. Chen, C.T., Nguyen, C.V., Wang, Z.Y., Bando, Y., Yamauchi, Y., Bazziz, M.T.S.,

515   Fatehmulla, A., Farooq, W.A., Yoshikawa, T., Masuda, T., 2018. Hydrogen

516   peroxide assisted selective oxidation of 5-hydroxymethylfurfural in water under

517   mild conditions. ChemCatChem 10, 361-365.

518   10. Chen, L., Chen, R., Fu, S., 2014. Preliminary exploration on pretreatment with

519   metal chlorides and enzymatic hydrolysis of bagasse. Biomass Bioenergy 71, 311-

520   317.

521   11. Chung, N.H., Cuong, T.D., Van Lieu, N., Hoang, P.H., 2018. Influence of the

522   acidity of solid catalyst HSO$_3$-ZSM-5 on the hydrolysis of pretreated corncob. RSC

523   Adv. 8, 41776-41781.

524   12. Cotana, F., Cavalaglio, G., Gelosia, M., Coccia, V., Petrozzi, A., Ingles, D.,

525   Pompili, E., 2015. A comparison between SHF and SSSF processes from cardoon

526   for ethanol production. Ind. Crops Prod. 69, 424-432.

527   13. De Bari, I., Liuzzi, F., Villone, A., Braccio, G., 2013. Hydrolysis of concentrated

528   suspensions of steam pretreated *Arundo donax*. Appl. Energy 102, 179-189.

529   14. Di Fidio, N., Antonetti, C., Raspolli Galletti, A.M., 2019a. Microwave-assisted

530   cascade exploitation of giant reed (*Arundo donax* L.) to xylose and levulinic acid

531   catalysed by ferric chloride. Bioresour. Technol. 293, 122050-122058.

532   15. Di Fidio, N., Liuzzi, F., Mastrolitti, S., Albergo, R., De Bari, I., 2019b. Single cell

533   oil production from undetoxified *Arundo donax* L. hydrolysate by

534   *Cutaneotrichosporon curvatus*. J. Microbiol. Biotechnol. 29, 256-267.

535   16. Di Fidio, N., Raspolli Galletti, A.M., Fulignati, S., Licursi, D., Liuzzi, F., De Bari,

536   I., Antonetti, C., 2020. Multi-Step Exploitation of Raw *Arundo donax* L. for the

537   Selective Synthesis of Second-Generation Sugars by Chemical and Biological

538   Route. Catalysts 10, 79-102.

539   17. Dragoni, F., Ragaglini, G., Corneli, E., Nassi o Di Nasso, N., Tozzini, C., Cattani,

540   S., Bonari, E., 2015. Giant reed (*Arundo donax* L.) for biogas production: land use

541   saving and nitrogen utilisation efficiency compared with arable crops. Ital. J. Agron.

542   10, 192-201.

543   18. Dutta, S., Kim, J., Ide, Y., Kim, J.H., Hossain, M.S.A., Bando, Y., Yamauchi, Y.,

544   Wu, K.C.W., 2017. 3D network of cellulose-based energy storage devices and

545   related emerging applications. Mater. Horiz. 4, 522-545.

546   19. Fulignati, S., Antonetti, C., Licursi, D., Pieraccioni, M., Wilbers, E., Heeres, H.J.,

547   Raspolli Galletti, A.M., 2019. Insight into the hydrogenation of pure and crude

548   HMF to furan diols using Ru/C as catalyst. Appl. Catal. A-Gen. 578, 122-133.

549   20. Huang, C., Lin, W., Lai, C., Li, X., Jin, Y., Yong, Q., 2019. Coupling the post-

550   extraction process to remove residual lignin and alter the recalcitrant structures for

551   improving the enzymatic digestibility of acid-pretreated bamboo residues.

552   Bioresour. Technol. 285, 121355-121363.

553   21. Jeong, H., Jang, S.K., Hong, C.Y., Kim, S.H., Lee, S.Y., Lee, S.M., Choi, J.W.,

554   Choi, I.G., 2017. Levulinic acid production by two-step acid-catalyzed treatment of

555   *Quercus mongolica* using dilute sulfuric acid. Bioresour. Technol. 225, 183-190.

556   22. Kamireddy, S.R., Li, J., Tucker, M., Degenstein, J., Ji, Y., 2013. Effects and

557   mechanism of metal chloride salts on pretreatment and enzymatic digestibility of

558   corn stover. Ind. Eng. Chem. Res. 52, 1775-1782.

559   23. Kang, K.E., Park, D.H., Jeong, G.T., 2013. Effects of inorganic salts on

560   pretreatment of *Miscanthus* straw. Bioresour. Technol. 132, 160-165.

561   24. Kohli, K., Prajapati, R., Sharma, B.K., 2019. Bio-based chemicals from renewable

562   biomass for integrated biorefineries. Energies 12, 233-272.

563   25. Kumar, V., Yadav, S.K., Kumar, J., Ahluwalia, V., 2019. A critical review on

564   current strategies and trends employed for removal of inhibitors and toxic materials

565   generated during biomass pretreatment. Bioresour. Technol. 299, 122633-122640.

566 26. Liao, Y.T., Matsagar, B.M., Wu, K.C.W., 2018. Metal–organic framework (MOF)-

567   derived effective solid catalysts for valorization of lignocellulosic biomass. ACS

568   Sustain. Chem. Eng. 6, 13628-13643.

569 27. Liao, Y.T., Van Chi, N., Ishiguro, N., Young, A.P., Tsung, C.K., Wu, K.C.W.,

570   2020. Engineering a homogeneous alloy-oxide interface derived from metal-organic

571   frameworks for selective oxidation of 5-hydroxymethylfurfural to 2, 5-

572   furandicarboxylic acid. Appl. Catal. B 270, 118805-118816.

573 28. Licursi, D., Antonetti, C., Bernardini, J., Cinelli, P., Coltelli, M.B., Lazzeri, A.,

574   Martinelli, M., Galletti, A.M.R., 2015. Characterization of the *Arundo donax* L.

575   solid residue from hydrothermal conversion: Comparison with technical lignins and

576   application perspectives. Ind. Crops Prod. 76, 1008-1024.

577 29. Licursi, D., Antonetti, C., Fulignati, S., Giannoni, M., Raspolli Galletti, A.M.,

578   2018a. Cascade strategy for the tunable catalytic valorization of levulinic acid and γ-

579   valerolactone to 2-methyltetrahydrofuran and alcohols. Catalysts 8, 277-292.

580 30. Licursi, D., Antonetti, C., Mattonai, M., Pérez-Armada, L., Rivas, S., Ribechini, E.,

581   Raspolli Galletti, A.M., 2018b. Multi-valorisation of giant reed (*Arundo Donax* L.)

582   to give levulinic acid and valuable phenolic antioxidants. Ind. Crops Prod. 112, 6-

583   17.

584 31. Lin, Q., Yan, Y., Wang, X., Cheng, B., Meng, L., Yue, F., Lan, W., Sun, R., Ren, J.,

585   2019. Corncob Biorefinery for Platform Chemicals and Lignin Coproduction: Metal

586   Chlorides as Catalysts. ACS Sustain. Chem. Eng. 7, 5309-5317.

587 32. Lin, W., Xing, S., Jin, Y., Lu, X., Huang, C., Yong, Q., 2020. Insight into

588   understanding the performance of deep eutectic solvent pretreatment on improving

589   enzymatic digestibility of bamboo residues. Bioresour. Technol. 306, 123163-

590   123171.

591 33. Liu, L., Sun, J., Cai, C., Wang, S., Pei, H., Zhang, J., 2009. Corn stover pretreatment

592   by inorganic salts and its effects on hemicellulose and cellulose degradation.

593   Bioresour. Technol. 100, 5865-5871.

594 34. Loow, Y.L., Wu, T.Y., Tan, K.A., Lim, Y.S., Siow, L.F., Md. Jahim, J.,

595   Mohammad, A.W., Teoh, W.H., 2015. Recent advances in the application of

596   inorganic salt pretreatment for transforming lignocellulosic biomass into reducing

597   sugars. J. Agric. Food Chem. 63, 8349-8363.

598 35. López-Linares, J.C., Romero, I., Moya, M., Cara, C., Ruiz, E., Castro, E., 2013.

599   Pretreatment of olive tree biomass with $FeCl_3$ prior enzymatic hydrolysis.

600   Bioresour. Technol. 128, 180-187.

601 36. Matsagar, B.M., Hsu, C.Y., Chen, S.S., Ahamad, T., Alshehri, S.M., Tsang, D.C.,

602   Wu, K.C.W., 2020. Selective hydrogenation of furfural to tetrahydrofurfuryl alcohol

603   over a Rh-loaded carbon catalyst in aqueous solution under mild conditions. Sustain.

604   Energ. Fuels 4, 293-301.

605 37. Mishra, A., Ghosh, S., 2020. Saccharification of kans grass biomass by a novel

606   fractional hydrolysis method followed by co-culture fermentation for bioethanol

607   production. Renew. Energy 146, 750-759.

608 38. Rodriguez Quiroz, N., Norton, A.M., Nguyen, H., Vasileiadou, E., Vlachos, D.G.,

609   2019. Homogeneous Metal Salt Solutions for Biomass Upgrading and Other Select

610   Organic Reactions. ACS Catal. 9, 9923-9952.

611   39. Saha, B.C., Kennedy, G.J., Bowman, M.J., Qureshi, N., Dunn, R.O., 2019. Factors

612   affecting production of itaconic acid from mixed sugars by *Aspergillus terreus*.

613   Appl. Biochem. Biotechnol. 187, 449-460.

614   40. Shatalov, A.A., Pereira, H., 2012. Xylose production from giant reed (*Arundo donax*

615   L.): modeling and optimization of dilute acid hydrolysis. Carbohydr. Polym. 87,

616   210-217.

617   41. Silvester, L., Ramos, F., Thuriot-Roukos, J., Heyte, S., Araque, M., Paul, S.,

618   Wojcieszak, R., 2019. Fully integrated high-throughput methodology for the study

619   of Ni- and Cu-supported catalysts for glucose hydrogenation. Catal. Today 338, 72-

620   80.

621   42. Tempelman, C., Jacobs, U., Hut, T., de Pina, E.P., van Munster, M., Cherkasov, N.,

622   Degirmenci, V., 2019. Sn exchanged acidic ion exchange resin for the stable and

623   continuous production of 5-HMF from glucose at low temperature. Appl. Catal. A-

624   Gen. 588, 117267-117275.

625   43. Van Nguyen, C., Boo, J.R., Liu, C.H., Ahamad, T., Alshehri, S.M., Matsagar, B.M.,

626   Wu, K.C.W., 2020. Oxidation of biomass-derived furans to maleic acid over

627   nitrogen-doped carbon catalysts under acid-free conditions. Catal. Sci. Technol. 10,

628   1498-1506.

629   44. Wang, C., Zhang, Q., Chen, Y., Zhang, X., Xu, F., 2018a. Highly efficient

630   conversion of xylose residues to levulinic acid over $FeCl_3$ catalyst in green salt

631   solutions. ACS Sustain. Chem. Eng. 6, 3154-3161.

632   45. Wang, L., Templer, R., Murphy, R.J., 2012. High-solids loading enzymatic

633   hydrolysis of waste papers for biofuel production. Appl. Energy 99, 23-31.

634   46. Wang, S., Lv, M., Yang, J., Zhou, Y., Xu, B., 2018b. Effects and mechanism of

635   metal ions on enzymatic hydrolysis of wheat straw after pretreatment. Bioresources

636   13, 2617-2631.

637   47. Wang, W., Mittal, A., Pilath, H., Chen, X., Tucker, M.P., Johnson, D.K., 2019.

638   Simultaneous upgrading of biomass-derived sugars to HMF/furfural via

639   enzymatically isomerized ketose intermediates. Biotechnol. Biofuels 12, 1-9.

640   48. Zhang, J., Wang, Y., Zhang, L., Zhang, R., Liu, G., Cheng, G., 2014. Understanding

641   changes in cellulose crystalline structure of lignocellulosic biomass during ionic

642   liquid pretreatment by XRD. Bioresour. Technol. 151, 402-405.

643   49. Zhang, T., Kumar, R., Tsai, Y.D., Elander, R.T., Wyman, C.E., 2015. Xylose yields

644   and relationship to combined severity for dilute acid post-hydrolysis of

645   xylooligomers from hydrothermal pretreatment of corn stover. Green Chem. 17,

646   394-403.

647   50. Zheng, X., Zhi, Z., Gu, X., Li, X., Zhang, R., Lu, X., 2017. Kinetic study of

648   levulinic acid production from corn stalk at mild temperature using $FeCl_3$ as

649   catalyst. Fuel 187, 261-267.

650

651

652

653

654

655

656

657

658 **Captions for Figures**

659 **Fig. 1.** Response surface of glucose yield (mol%) as a function of: A) reaction time

660 (min) and FeCl$_3$ amount (wt%) calculated for the intermediate temperature ($x_1 = 0$); B)

661 temperature (°C) and FeCl$_3$ amount (wt%) calculated for the intermediate reaction time

662 ($x_2 = 0$); C) temperature (°C) and reaction time (min) calculated for the intermediate

663 FeCl$_3$ amount ($x_3 = 0$).

664 **Fig. 2.** Kinetics of enzymatic hydrolysis of the CRR (black curves) and raw giant reed

665 (white curves).

666 **Fig. 3.** Kinetic of LA and FA synthesis in the microwave-assisted FeCl$_3$-catalysed

667 hydrolysis.

668 **Fig. 4.** Mass balance flow diagram of the chemical and enzymatic processes from CRR.

669

670

671

672

673

674

675

676

677

678

679

680

681

682   **Table 1**

683   Chemical composition of solid residues (wt% on dry matter).

Solid residue	Glucan	Acid-insoluble lignin	Acid-soluble lignin	Ash	Other compounds
CRR[a]	50.0 ± 1.7	34.4 ± 1.1	0.4 ± 0.2	ash 3.0 ± 0.2	11.6 ± 3.2
Post-EHR[b]	38.2 ± 0.4	44.5 ± 0.9	0.1 ± 0.0	ash 3.8 ± 0.3	13.4 ± 1.6
Post-CHR[c]	40.1 ± 0.8	55.5 ± 0.7	0.1 ± 0.0	4.3 ± 0.5	-
LRR[d]	8.0 ± 0.3	85.3 ± 1.7	-	ash 6.7 ± 0.2	-

684   [a] Cellulose-rich residue; [b] Post-enzymatic hydrolysis residue; [c] Post-chemical hydrolysis

685   residue; [d] Lignin-rich residue.

686

687

688

689

690

691

692

693

694

695

696

697

698

699

700 **Table 2**

701 Experimental design matrix defining the operating conditions for glucose production

702 and values of the response variable.

| Run | Dimensionless normalised variables | | | Dimensional variables | | | Dependent variable |
	x_1	x_2	x_3	T (°C)	t (min)	Cat (wt%)	Glucose yield[a] (mol%)
1	-1	-1	0	120	5	2.5	0.0
2	-1	1	0	120	65	2.5	7.1
3	1	-1	0	190	5	2.5	1.8
4	1	1	0	190	65	2.5	0.0
5	-1	0	-1	120	35	0.2	2.3
6	-1	0	1	120	35	4.8	9.1
7	1	0	-1	190	35	0.2	18.1
8	1	0	1	190	35	4.8	0.0
9	0	-1	-1	155	5	0.2	9.5
10	0	-1	1	155	5	4.8	31.3
11	0	1	-1	155	65	0.2	18.8
12	0	1	1	155	65	4.8	16.7
13	0	0	0	155	35	2.5	37.0
14	0	0	0	155	35	2.5	39.8
15	0	0	0	155	35	2.5	40.1

703   [a] Yield respect to moles of glucan in the cellulose-rich residue.

704

705

706

707   **Table 3**

708   Results of the experimental design in terms of products concentrations (g/L), mass

709   balance (wt%) and CRR solubilisation (wt%).

Run	Glu[1] (g/L)	HMF[2] (g/L)	LA[3] (g/L)	FA[4] (g/L)	Mass balance (wt%)	CRR solubilisation (wt%)
1	0.0	0.0	0.0	1.7	97.7	5.9
2	3.9	0.0	0.0	1.8	95.7	14.6
3	1.0	0.0	18.4	9.7	70.7	59.5
4	0.0	0.0	21.1	9.5	70.4	60.2
5	1.3	0.0	0.0	1.6	98.6	8.1
6	5.1	0.0	0.0	2.3	92.0	21.1
7	10.1	2.9	6.5	5.2	71.9	56.5
8	0.0	0.0	22.7	10.0	72.1	60.6
9	5.3	0.4	0.0	1.8	95.9	16.0
10	17.3	1.2	2.2	3.5	96.2	33.4
11	10.5	0.7	0.0	1.9	97.1	21.5
12	9.3	0.7	21.2	11.3	83.6	59.5
13	20.5	1.2	3.4	3.8	90.5	43.6
14	22.1	1.2	3.8	3.9	92.4	43.2
15	22.2	1.4	3.6	3.5	83.3	51.2

710   [1] Glucose; [2] 5-hydroxymethylfurfural; [3] Levulinic acid; [4] Formic acid.

711

712

713

714

715

716

717

718

719 **Table 4**

720 Coefficients of the model equation and statistical parameters.

Regression coefficients					
Linear coefficients		Interaction coefficients		Quadratic coefficients	
β_0	38.967^a	β_{12}	-2.225	β_{11}	-0.526^b
β_1	0.175	β_{13}	-6.225^c	β_{22}	-24.221^b
β_2	0.000	β_{23}	-5.975^c	β_{33}	-7.371^c
β_3	1.050				
Model					
R^2	0.950	Ad. R^2	0.860	F	10.5

721 [a] Significance at 99%; [b] Significance at 95%; [c] Significance at 90%; F = Fisher value.

722

723

724

725

726

727
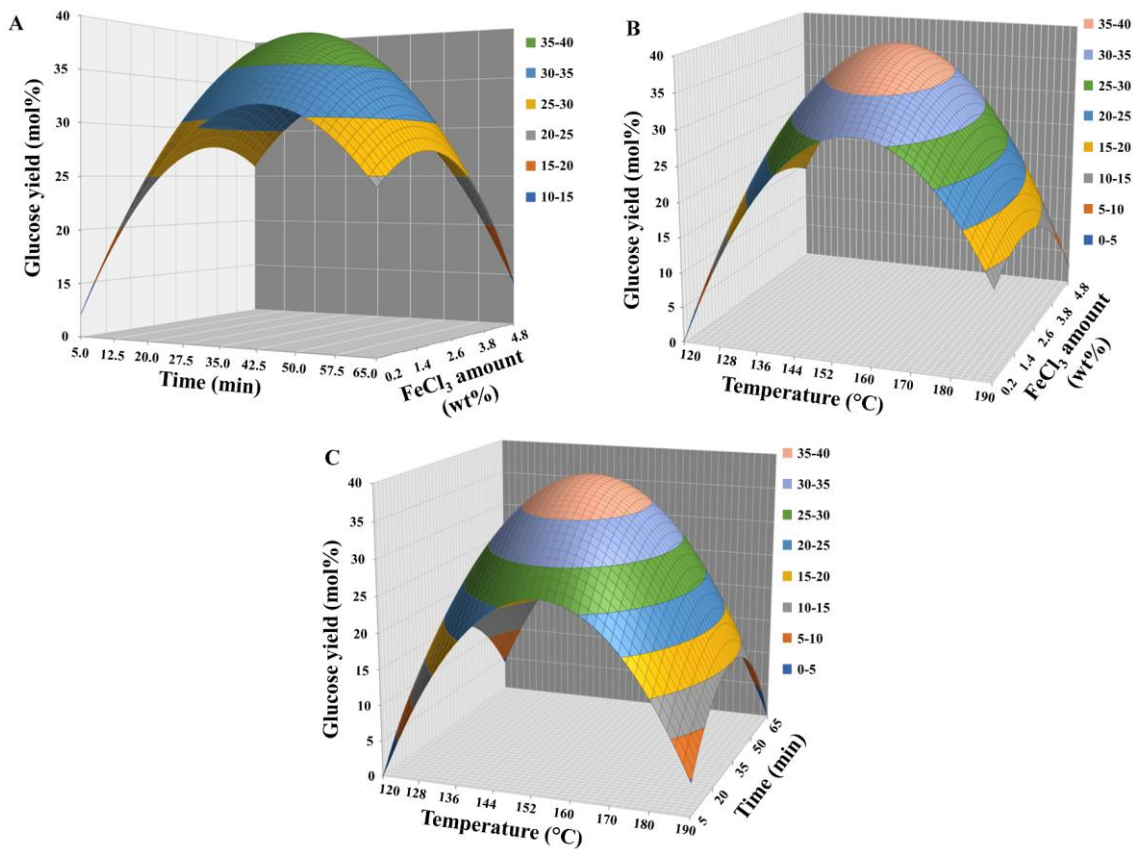
728

729

730

Figure 1

731
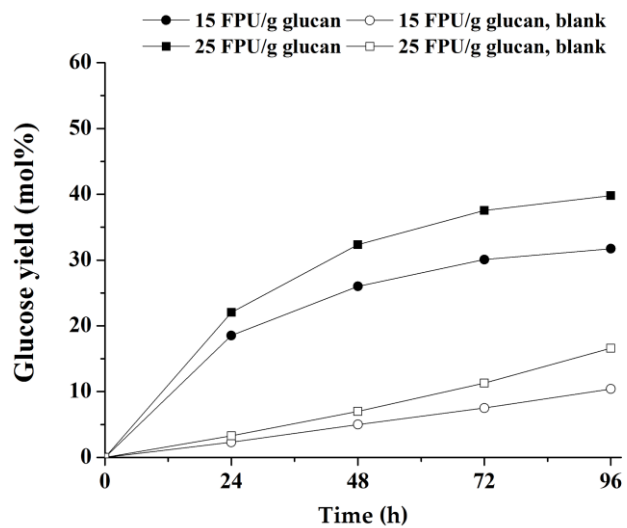
732

733

734

735

736

737

738

739

740

741

742

743

34

Figure 2

744

745

746

747

748

749

750

751

752

753

754

755

756

757

758

759

760

Figure 3

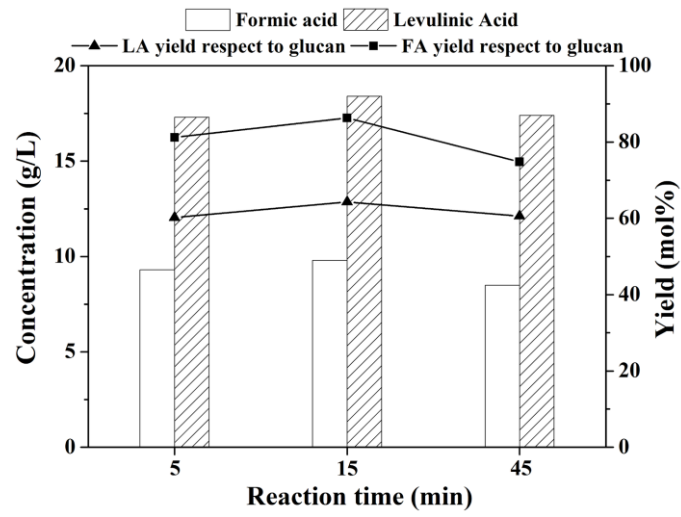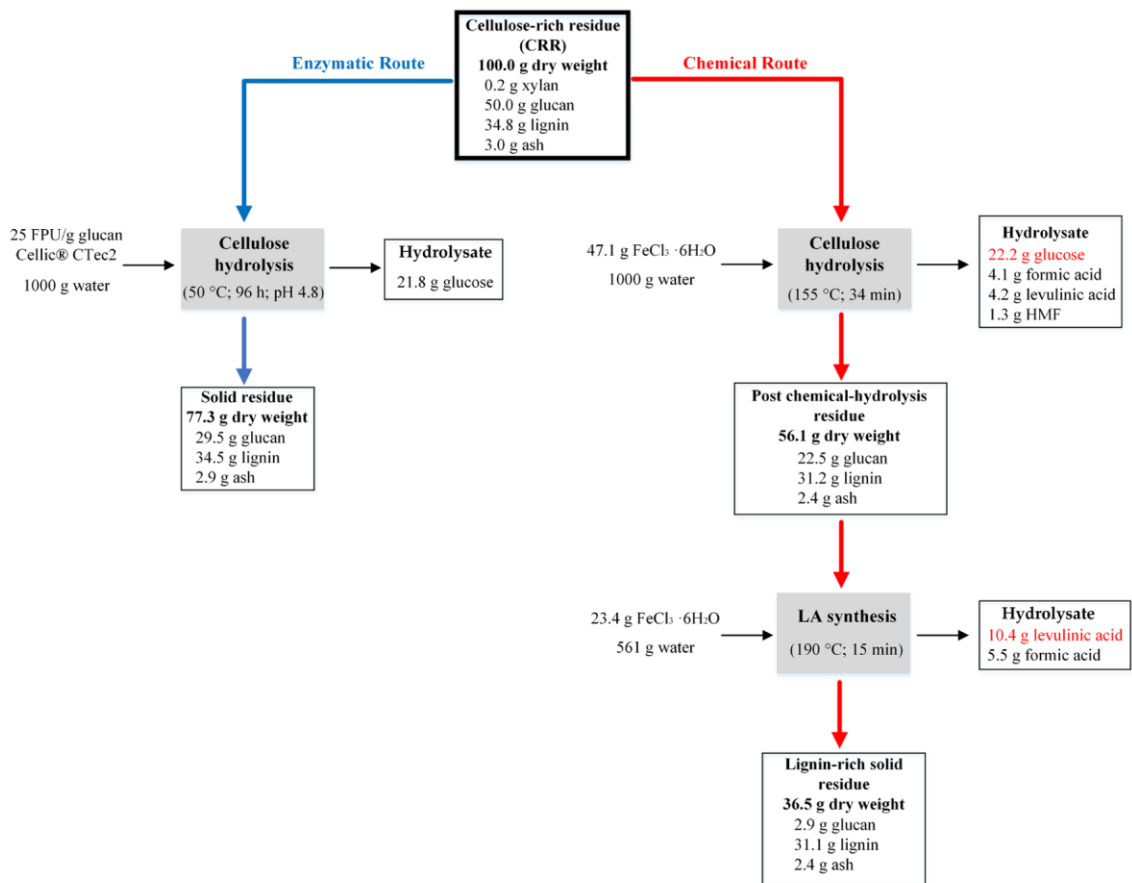761

762

763

764

765

766

767

768

769

770

771

772

773

774

775

776

36

777

778   **Figure 4**